



Influence of oval-shaped tube on falling film flow characteristics on horizontal tube bundle

Lincong Luo^{a,b}, Guanmin Zhang^a, Jihong Pan^a, Maocheng Tian^{a,*}

^a*School of Energy and Power Engineering, Shandong University, No.19723 Jingshi Road, Jinan 250061, P.R. China, Tel. +86 531 88395421; email: tianmc65@sdu.edu.cn*

^b*National Urban Energy Measurement Center (Chongqing), No. 1 Yangliubei Road, Yubei District, Chongqing 401123, P.R. China*

Received 4 October 2013; Accepted 10 March 2014

ABSTRACT

Falling liquid film flow on a horizontal tube is an important process which plays an important role in heat transfer in heat exchangers. The aim of the present study is to investigate experimentally the effect of the oval-shaped tube on flow characteristics of liquid falling film. The effects of the tube type, Reynolds number, and intertube spacing on the falling film flow modes, dimensionless wavelength, and film thickness for a horizontal tube bundle were studied. Compared with the circular tube, the transitional Reynolds number of the shaped tube is smaller for the oval-shaped tube. The falling wavelength increases with the decrease of Reynolds number and firstly increases then tends towards stability with increasing of intertube spacing. The falling wavelength of the oval-shaped tube is smaller than that of the circular tube. The minimum value of the film thickness appears approximately at the angular position of 135° for the oval-shaped tube, while the angular position of the circular is 105°. Finally, these conclusions obtained in this article provide a valuable reference to the application of the shaped tube in the falling film evaporator for the seawater desalination system.

Keywords: Oval-shaped tube; Falling film flow; Flow mode; Wavelength; Experimental study

1. Introduction

Low-temperature multi-effect distillation (LT-MED) is a technology with a promising application prospect that has a better freshwater production capacity. Over the last decade, as the most efficient thermal desalination processes, the LT-MED has caught the attention of lots of researchers and has been studied intensively. The horizontal tube falling film evaporation is a key process in the LT-MED, which is composed of horizontal tube bundles, condensing steam inside the tube

and film evaporation outside the tube. This falling film evaporator has advantages over the conventional flooded evaporator. These advantages are: (a) the pressure drop of the liquid flowing over the tubes is negligible, (b) the quantity of cooling liquid required is small, and (c) the heat transfer coefficients are high [1]. Falling film evaporators have been widely applied in several industrial processes (i.e. desalination and freshwater treatment industry, chemical and petrochemical industries, refrigeration, food and dairy industries, etc.).

The heat transfer process of horizontal tube falling film evaporation can be divided into three main parts,

*Corresponding author.

this includes: condensation heat transfer inside the tube, heat conduction through the tube wall, and evaporative heat transfer outside the tube. The evaporation heat transfer coefficient is affected mainly by the flow condition outside the horizontal tubes. In order to better understand the mechanism of heat transfer of the falling film evaporation, it is necessary to study the flow mode between the tubes and the liquid film on the tube.

In falling film heat exchangers, basically three different modes of flow between the tubes have idealized and described by Mitrovic [2], i.e. discrete droplets, liquid column (or jet), and continuous liquid sheet, as shown in Fig. 1. Each of these flow modes depends on the flow rate, the tube spacing, and the physical properties of the liquid. Hu and Jacobi [3] carried out an experimental study of the flow characteristics and mode transitions of the falling film on horizontal tube and subdivided the flow mode into droplets, droplet-jet, inline jet, staggered jet, jet-sheet, and sheet mode. A simplified flow regime map for the falling film mode transitions in the $Re-Ga^{1/4}$ space was developed by the experimental results. Mitrovic [2] investigated experimentally the heat transfer and the flow mode from a horizontal heated tube for a falling subcooled liquid film. The experimental results also showed that the transition from the droplet mode to the jet mode occurred at Reynolds numbers between 150 and 200, while the transition from the jet mode to the sheet mode occurred at Reynolds between 315 and 600 for water as a working medium.

Taylor instability plays an important role in the droplet and jet modes. The distance between two neighboring droplets or jets falling from the tube has a fixed value. This distance is defined as the falling wavelength, λ , as shown in Fig. 1. Many researchers have considered the falling wavelength as an

important parameter besides the flow modes and film thickness of the falling film flow. The first report about the falling wavelength was discovered in the work of Bellman and Pennington [4] for inviscid, incompressible fluids. They found the critical and most dangerous Taylor wavelengths to be given by:

$$\lambda_c = 2\pi \sqrt{\frac{\sigma}{g(\rho_L - \rho_V)}}, \lambda_d = \sqrt{3}\lambda_c \quad (1)$$

where σ , g , ρ_L , and ρ_V are surface tension, the gravity acceleration, the density of the liquid and vapor, respectively.

Armbruster and Mitrovic [5] developed the following correlation of the falling wavelength for the jet mode by considering the effect of flow rate for water and isopropanol as a working medium. The maximum relative error of the correlation is within $\pm 7.5\%$.

$$\lambda = \frac{2\pi\sqrt{2}}{\sqrt{\frac{g(\rho_L - \rho_V)}{\sigma} \left(1 + \left(\frac{Re^{1/2}}{Ga^{1/4}}\right)^{0.8}\right) + \frac{2}{d^2}}} \quad (2)$$

where Ga is modified Galileo number, $\rho\sigma^3/(g\mu^4)$, and d is the diameter of the test tube.

Mohamed [6] experimentally studied the mode transform and wavelength of falling film flow outside a horizontal fluted tube for four fluids, including water, a mixture of 50% glycol and 50% water, glycol, and oil. Hu and Jacobi [7] investigated the influence of mass flow rate, the diameter of the tube and intertube spacing on the falling wavelength by experimental observations. They developed a semi-empirical correlation of the dimensionless wavelength λ^* with an RMS error less than 8.3%, as follows:

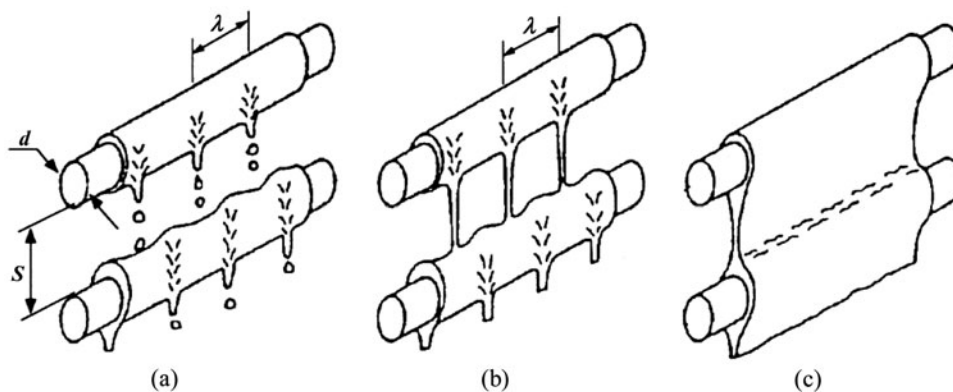


Fig. 1. Modes of liquid flow between two horizontal tubes: (a) droplet mode, (b) jet mode, and (c) sheet mode.

$$\lambda^* = \frac{0.836A - 0.836Re/Ga^{1/4}}{\left\{1 + \left(\frac{0.836A - 0.836Re/Ga^{1/4}}{0.75A - 85/Ga^{1/4}}\right)^2\right\}^{1/12}} \quad (3)$$

where

$$A = \frac{2\pi\sqrt{3}}{\sqrt{1 + 2/(d/\sqrt{\sigma/\rho g})^2}} \quad (4)$$

Maron-Moalem et al. [8] studied the influence of mass flow rate, surface tension, the tube diameter, and intertube spacing on the falling film flow on the horizontal tubes and measured the detach frequency of liquid drop and the falling wavelength. The results show that the falling wavelength decreases with the increase of the mass flow rate, and increases with increasing the detach frequency, the tube diameter, and intertube spacing. The influence of feeder height, the tube diameter, and intertube spacing on the falling wavelength for water and cooking oil was investigated by an experiment [9]. Wang et al. [10] experimentally studied flow patterns and mode transitions for falling films and found some interesting differences in the flow characteristics between the circular and flat tube. The effects of liquid supply method on falling film transitions between horizontal tubes are experimentally studied by Wang et al. [11], and the results show that the falling film mode transitions at large feeding height occur at higher Reynolds number than those at small feeding height.

Since the characteristics of falling films have drawn great attention, the researches have been conducted on the film thickness by both theoretical and practical approaches in the past years. Nusselt [12] first analyzed falling films and obtained the following expression for the falling film thickness by using integral method, assuming a continuous sheet flow from tube to tube and momentum effects in the falling films to be negligible.

$$\delta = \left(\frac{3\mu_L\Gamma}{\rho_L(\rho_L - \rho_V)g \sin \beta}\right)^{1/3} \quad (5)$$

where β is the circumferential angle measured from the top of a horizontal tube and Γ is the liquid flow rate per unit length on one side of the tube. With this definition, the film Reynolds number is given below:

$$Re = \frac{4\Gamma}{\mu} \quad (6)$$

Rogers and Goindi [13] carried out an experiment to study the film thickness of water laminar falling flow on a large diameter horizontal tube. They rewrote Eq. (5) in non-dimensional terms, and developed a new predicted correlation of the film thickness, as follows:

$$\left(\frac{\delta}{d}\right)_{\min} = 1.186Re^{1/3}Ar^{-1/3} \quad (7)$$

where Ar is Archimedes number, $g\rho^2d^3/\mu^2$.

While a considerable amount of studies focused on a circular cylinder for liquid falling film, the study of falling film flow on a non-circular cylinder has not received adequate attention. It needs to more details and extensive investigations to model the horizontal falling film behavior and clear the mechanism of flow enhancement especially for the case of the non-circular tube. Therefore, this paper presents an oval-shaped tube combined with the cross-section shape of circular and elliptical cylinders. The main objective of this present work is to perform a visualization experiment to investigate the effect of the non-circular enhanced tube on horizontal falling film behavior in falling film evaporators for LT-MED. This includes the flow mode transitions, film thickness, and the film wavelength. Detailed experimental data are obtained to provide a better understanding of the distribution characteristics of the flow mode and film thickness.

2. Experimental setup

A schematic diagram of the experimental test rig is shown in Fig. 2. The test rig was designed after considering several schemes described in the literature. The test rig mainly consists of the collecting tank, the circulating pump, the flowmeter, the constant-pressure tank, the distribution tube, the upper dummy tube, the test tube, the lower dummy tube, and many control valves. They are held in the middle by one metallic frame. The fluid in the collecting tank is circulated by a small pump to the constant-pressure tank through the flowmeter. The quantity of the fluid flow is controlled by a by-pass system via control valves. The fluid is then passed through a rotameter of a small or large measurement range, with an accuracy of 1.0% or 1.5%, to measure the volume flow rate of the fluid. The flow rate is measured with one of two rotameters, which are necessary to cover the desired ranges of mass flow. The flow rate is also checked by weight method, and the relative error between the rotameter and the weight method is within 1.0%.

The fluid leaves the distribution tube at the bottom through 2-mm-diameter holes spaced 10 mm apart

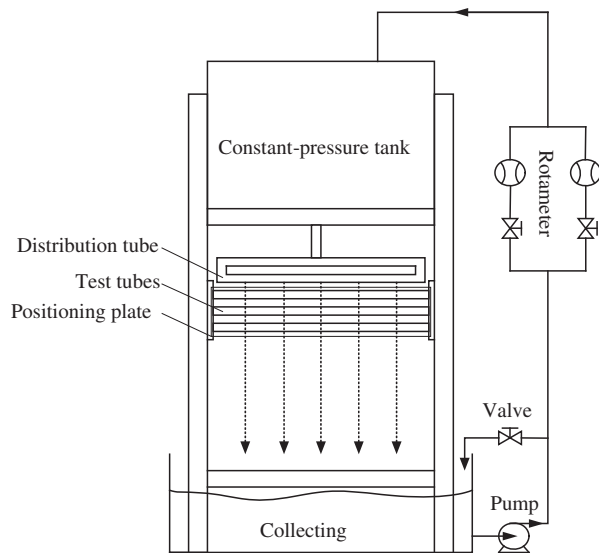


Fig. 2. Schematic diagram of experimental setup.

over a length of 200 mm. The fluid then falls from the distribution tube over the upper dummy tube. Consequently, the fluid falls freely from the upper dummy tube to the test tube, which has a diameter of 19 mm and a length of 600 mm. The test tube is supported by the edges with two positioning plate to control the intertube spacing, and the alignment of the test tube is adjusted carefully. The feeder height, between the distribution tube and the first test tube, is considered fixed at 12 mm.

Water is used as test fluids, as presented in Table 1. Digital Camera, Nikon (D7000, 16.2 Mega Pixels), is used to capture the falling film images through the experiments in the digital form. The liquid is impinged at the top part of the tube, with an initial mass flow rate of 2. The film flows along the tube under the common effect of gravity, viscous force, and surface tension at the liquid–vapor interface. Fig. 3 shows the physical models and body-fitted coordinates (the detail is described in Ref. [14]). The coordinate x is measured from the stagnation point of the tubes and y is measured normally from the surface wall to the fluid. The velocity components in the x - and y -direction are u and v , respectively.

The present analysis considers an oval-shaped tube which has the identical effective flow area with a

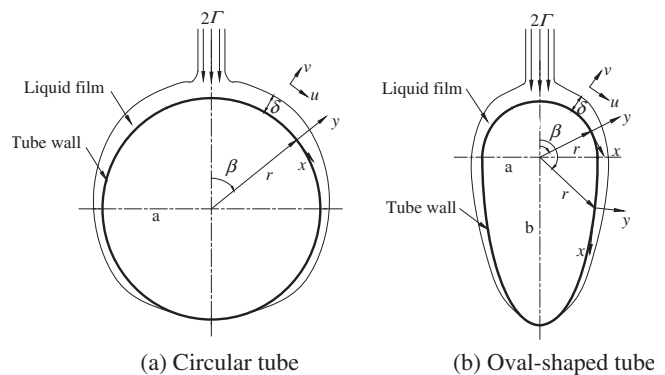


Fig. 3. Physical models and coordinate systems for test tubes.

circular tube of 19 mm in diameter. The cross-section of the oval-shaped tube is made up of upper semi-circle and lower semi-ellipse obtained by design optimization. The parameters of the two cylinders in the simulation are listed in Table 2, of which a is the radius of the circular tube, the radius of the upper semi-circle for the oval-shaped tube, respectively; b represents the radius of the bottom semi-circle for the ellipse semi-major axis.

3. Experimental procedure

Before the tests, care is taken to obtain a precise alignment of the horizontal tubes into a vertical array, so that axial uniformity of the film distribution can be kept for the falling film from tube to tube. All the tests were carried out at the atmospheric pressure and under the adiabatic condition. The surfaces of the metallic tubes were carefully polished by using crocus paper and cleaned by using acetone before the tests. The working fluid was deaerated before introduction into the experimental apparatus.

Two groups of tests were conducted with the test facility for testing the flow behavior of the oval-shaped or circular tube, respectively. Both groups are executed for the test fluid (water) with a constant temperature at different flow rates (Re up to 2000) when the intertube spacing S ranged from 5 to 20 mm. All measurements were made under steady state and isothermal ambient temperature conditions for the first

Table 1
The thermophysical properties of the fluid ($T = 25$ °C)

	$\rho/(\text{kg m}^{-3})$	$\mu/(\text{kg m}^{-1}\text{s}^{-1})$	$\sigma/(\text{N m}^{-1})$	$Ga^{0.25}$
Water	996.95	0.903×10^{-3}	0.07196	489

Table 2
Structure parameters for tubes

Tube type	a (mm)	b (mm)
Circular tube	9.50	–
Oval-shaped tube	6.08	18.22

Table 3

Parameters, the range, and typical uncertainties of measurement values

Dimensionless parameter	Experimental range	Estimated uncertainty
$Re = 4/\mu$	up to 2000	$\pm 2\%$
$d^* = d/\zeta$	0.019	$\pm 1\%$
$S^* = S/\zeta$	1.8–7.4	$\pm 4\%$
$\lambda^* = \lambda/\zeta$	–	$\pm 4\%$
β	30–150	$\pm 1\%$
δ	–	$\pm 8\%$

group. The test fluid was firstly circulated through the test rig for 0.5 h to reach the steady state conditions.

According to the work of Hou et al. [15], a displacement micrometer with a conducting probe was adopted to measure directly the film thickness around a horizontal tube. As a steady falling film was formed on the surfaces of the tubes, the film thickness was measured on the second tube. The film thickness was measured in a wide range of circumferential angles ($\beta = 30\text{--}150^\circ$). It is well known that the thickness of the liquid film is obtained from the distance between the gas–liquid interface of the liquid film and the surface of the tube. During the measurements, the liquid and air were considered as an electric and a dielectric medium, respectively. Based on the principle of the different conductivity characteristics of gas–liquid two-phase mediums, the probe of the displacement micrometer was used in the detection of the gas–liquid interface. A specially manufactured positioning frame was mounted on the test section, which could maintain the probe in the axial direction and apply the probe to different circumferential positions. As illustrated in Fig. 4, the displacement micrometer is connected to an electric circuit which is used to indicate the varying output voltages. As the probe contacts with the air, the electric circuit provides a low-level voltage output signal. On the contrary, a high-level voltage output signal is displayed when the probe just establishes contact with the liquid film. Accordingly, the gas–liquid interface of the liquid film is determined. Subsequently, the probe keeps moving in the liquid film along the radial direction until the probe just touches the tube. The surface of the tube is also determined. As a consequence, the thickness of the liquid film is the corresponding distance the probe advances. The arithmetic average of 10 times measurement results at the same location is regarded as the value of the film thickness.

All the instruments used to measure the experimental parameters have been thoroughly checked and

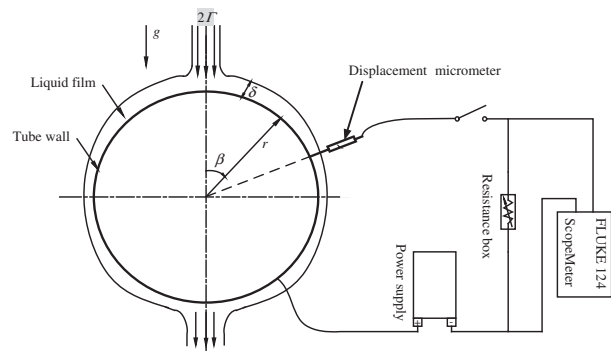


Fig. 4. Schematic of film thickness measurement system.

calibrated. All the signals of the instruments have been collected and recorded. The experimental uncertainties are shown in Table 3.

During the flow behavior experiments, digital images were recorded for each run at certain conditions. The digital camera was adjusted to capture the images at high-resolution mode. These high-resolution digital images were analyzed by using Photoshop software to measure the wavelengths. The number of pixels, of the wavelength, was measured from the image and compared with the number of pixels of the scale to calculate the dimensional value of the wavelength (in mm).

For mode transition experiments, the flow was increased and decreased slowly to obtain the different modes of flow by adjusting the control valve. The transition from one mode to another was observed visually, and the flow rate for each transition was recorded.

4. Results and discussion

A series of experiments were carried out in the case of circular and oval-shaped tube to measure the film thickness and the wavelength of the falling film. In addition, the evaluations of the mode transitions were observed for both the tubes. The circular tube is used as a reference to evaluate the effect of this shaped tube on the fluid flow behavior.

The experimental results showed only a small degree of hysteresis for increasing or decreasing the fluid flow rate; therefore, the effect of the hysteresis could be neglected. As there are five modes of flow and by neglecting the effect of the hysteresis, there are four falling film mode transitions. For the present study, the flow regime map was constructed to explain the effect of the geometry of the shaped tube on the mode transitions.

4.1. Effect of geometry of oval-shaped tube on the falling film mode transitions

Estimating the flow mode is very important, because the flow mode plays an important role in the calculations of the heat transfer coefficient and the design of the horizontal falling film heat exchangers.

The flow modes on the oval-shaped tube are similar to those on the circular tube, as shown in Fig. 5. They are sheet (a), sheet-jet (b), jet (column) (c), jet-droplet (d), and the droplet mode (e) with the decrease of film Reynolds number at a fixed intertube spacing. The wave and destabilization increase with the increase of film Reynolds number. The sheet and jet mode can make a continuous impingement disturbance to the next tube, while the drop mode just makes a small and discontinuous disturbance which has little effect on the thickness of the film and flow state.

Fig. 6 shows that a comparison of falling film flow mode of the oval-shaped and circular tube at $Re = 400$ and $S = 15$ mm. From the figure, it can be found that an obvious liquid bridge appears between the two jets for the oval-shaped tube, while the typical stagger jet mode presents on the circular tube. The cause of which is that the curvature of the lower part for

non-circular tube is smaller than that of the circular tube, which results in a larger gravity component in the flow direction and a larger flow rate of liquid film. The area of liquid gathered at the bottom of the oval-shaped tube is smaller than the circular, which results in the sheet and jet mode appeared at a lower Reynolds number. The essential characteristic of the shaped tube is that it has a gradual wall which is beneficial to the development of the falling film flow. Therefore, compared to the circular tube, the flow mode on the oval-shaped tube is more stable and the wave spread further along the tube surface, which indicates the oval-shaped tube has a better heat transfer performance than the circular tube. It is observed that the flow mode transition law of oval-shaped tube with the Reynolds number or intertube spacing is similar with that of the circular tube. However, the transitional Reynolds number of the shaped tube is smaller than that of the latter, as shown in Fig. 7. It gives a comparison of the transition boundaries obtained for the oval-shaped tube versus the plain, smooth tube of the same flow area. The primary difference is an enlargement of the zone in which jet-sheet mode exists; that is, the jet to jet-sheet transition occurs at

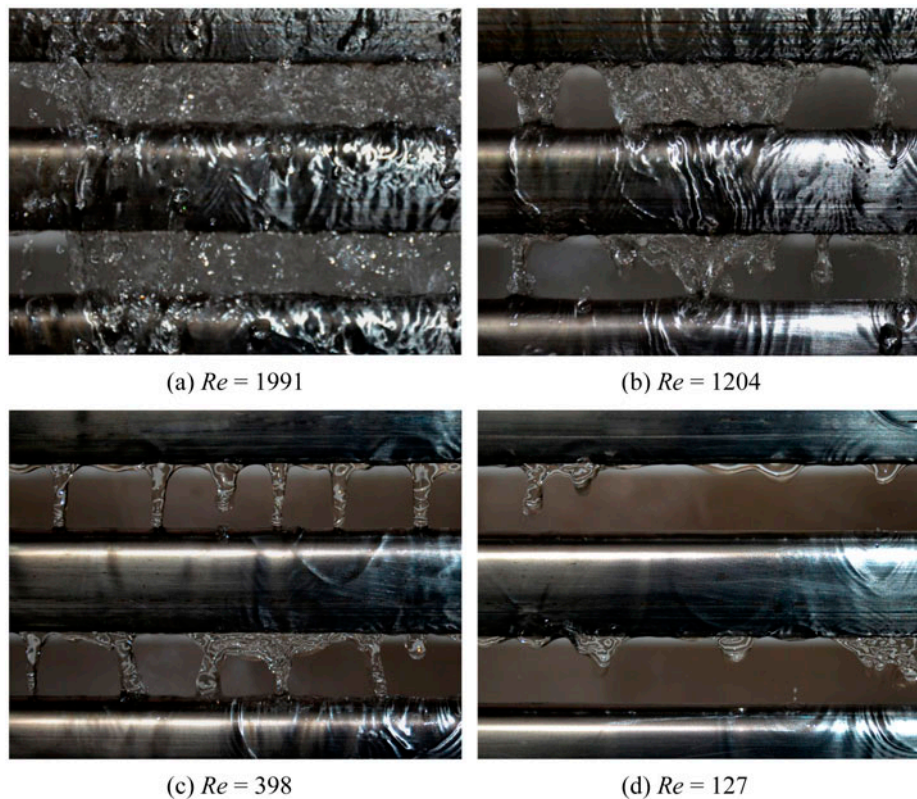
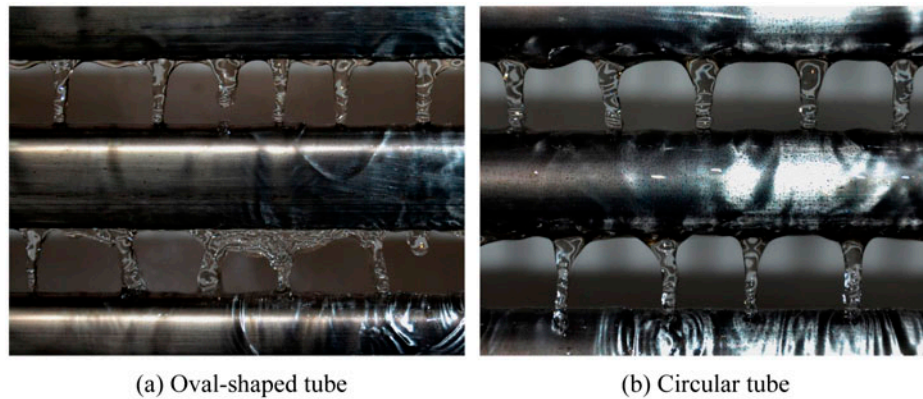
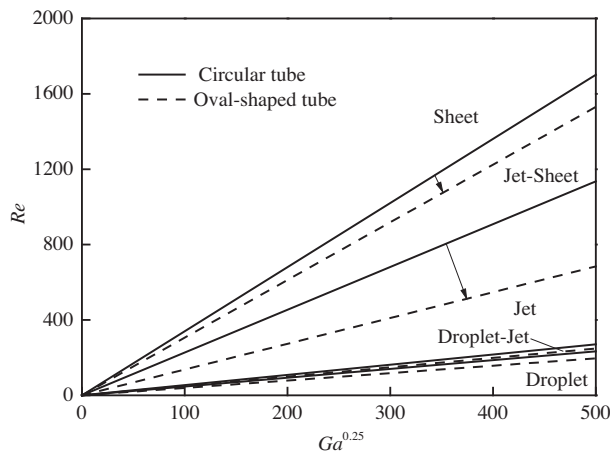


Fig. 5. The intertube flow modes of oval-shaped tube at different Reynolds number ($S = 15$ mm).



(a) Oval-shaped tube

(b) Circular tube

Fig. 6. Comparison of falling film flow mode of the oval-shaped and circular tube ($Re \approx 400$).Fig. 7. Flow mode transition maps for the circular and oval-shaped tube ($S = 15$ mm).

lower film Reynolds numbers, while the jet-sheet to sheet transition occurs at somewhat higher Reynolds numbers. In practice, this means that an evaporating falling film will tend to stay in the advantageous jet-sheet mode down to lower mass flow rates on oval-shaped tubes than on an array of circular tubes.

Fig. 8 describes the influence of intertube spacing on flow mode profiles for the oval-shaped tube, showing that the different flow mode with the variation of intertube spacing. The liquid jet cannot develop fully along the gravity direction, and the flow trend along the axis of the tube is obvious when the intertube spacing is small. So, the spacing between the neighboring jets is small, even some jets develop into a part sheet. According to the momentum theorem, $Ft = mv$, it means that the impact force is direct proportion to the falling velocity. The falling velocity of liquid is small at a small intertube spacing, which results in a

small impingement disturbance in the liquid film along the flow direction. The greater intertube spacing leads to greater free falling distance of the liquid and the larger impingement velocity of fluid upon the tube wall, which makes the stagnation zone at the upper semi-circle relatively more extensive and the impingement disturbance stranger. However, too big intertube spacing will lead to a large volume of falling film evaporator and the much thinner liquid jet even resulted in the fracture of the jet when the intertube spacing is larger than a certain value.

4.2. Effect of geometry of oval-shaped tube on the falling film wavelength

As one of the most important flow characteristics, the wavelength of the falling film is defined as the spacing between two neighboring jets or droplets. The dimensionless wavelength, λ^* , is defined as that falling film wavelength divided by the capillary constant, as follows:

$$\lambda^* = \lambda/\xi, \text{ where } \xi = \sqrt{\sigma/(g\rho_L)} \quad (8)$$

The variation of the falling wavelength of the oval-shaped tube with respect to the intertube spacing is indicated in Fig. 9. The wavelength increases with the intertube spacing S , and the growth rate decreases. When the intertube spacing increases over a certain value, the growth rate of wavelength is very small. This is because the intertube spacing has an important role in the wavelength. That means, liquid jet cannot develop fully along the gravity direction, and the flow trend along the axis of the tube is obvious when the intertube spacing is small. With the increase of the intertube spacing, the development trend of the liquid

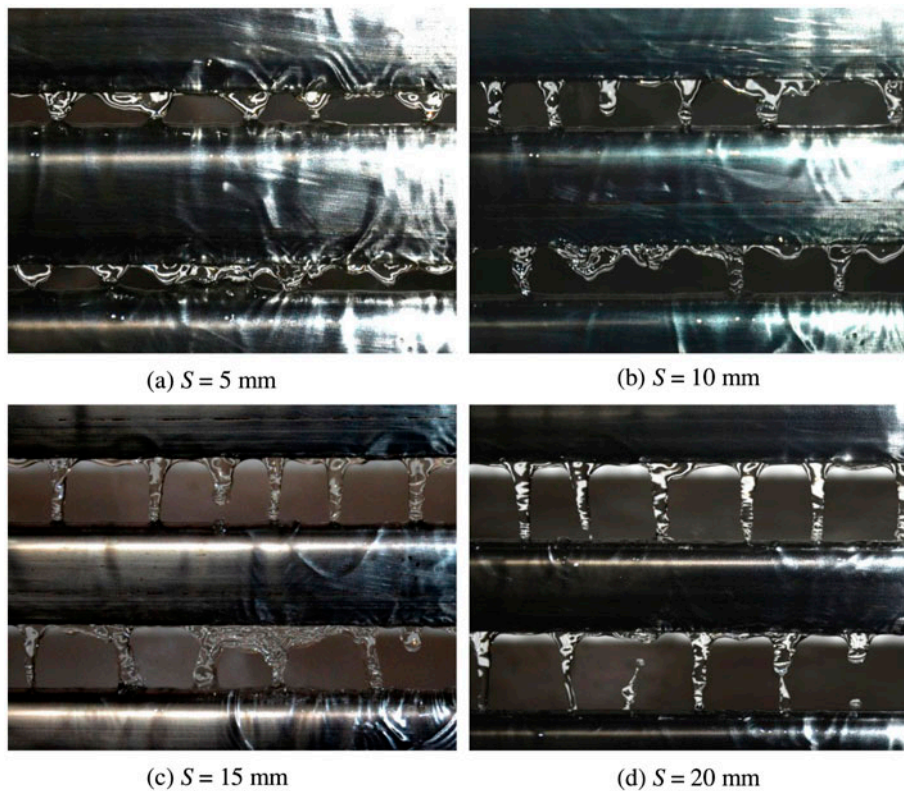


Fig. 8. Intertube flow mode of the oval-shaped tube at different intertube spacing ($Re = 398$).

jet along the gravity direction increases gradually and the axis movement weakens, which results in the larger wavelength. However, the liquid jets are stretched fully and the axis movement is almost disappeared after an enough intertube spacing, leading to a deterioration of the influence of intertube spacing on the wavelength, which means that the wavelength tends

to a stable value with the increase of intertube spacing.

To validate the present experiment, the experimental results are compared with previous semi-empirical correlations developed by Armbruster and Mitrovic [5] and Hu and Jacobi [7] under similar conditions in literature. Fig. 10 describes this comparison for the circular and oval-shaped tube at $S = 5$ mm, showing that the maximum relative is 10% for both the Eq. (2) and (3) which indicates that the experimental results are reliable. It is also noticed that the wavelength decreases as the Reynolds number increases, and the downtrend is more evident at low Reynolds number than at high Reynolds number. It is interesting to find that the value of falling wavelength of the oval-shaped tube is 6.66% smaller than that of the circular tube at an intertube spacing of 5 mm. The main reason is that the influence of the cross-section of the test tube on the falling flow of the fluid is different. That is, the bottom of the oval-shaped tube is smaller than the circular tube, which is helpful to the movement of the fluid along the surface of the former. Because of the larger curvature of the lower part, the axis movement is stranger outside the circular tube by the action of the surface tension. Therefore, the cross-section of the

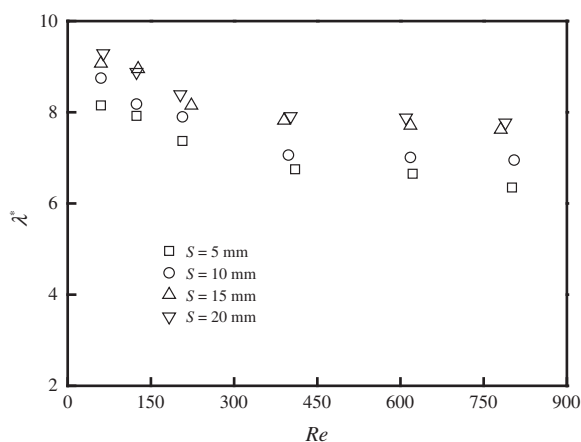


Fig. 9. Variations of falling film wavelength of the oval-shaped tube with intertube spacing.

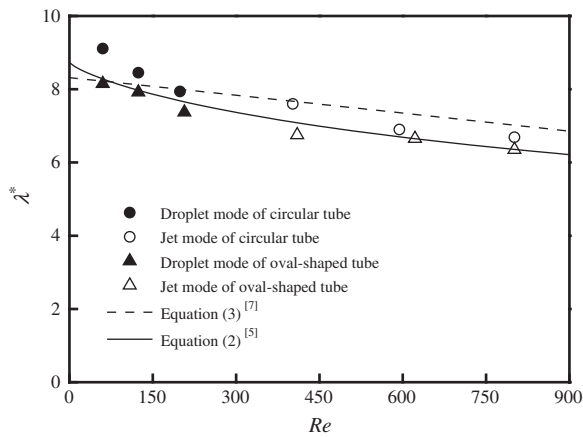


Fig. 10. Comparison of experimental falling film wavelength with correlation of Hu and Jacobi ($S = 5$ mm).

test tube has an important role in the falling film flow, and the wavelength of the oval-shaped tube is smaller than the circular tube.

4.3. Effect of geometry of oval-shaped tube on the film thickness

Film thickness was experimentally measured for the test tubes in a wide range of Reynolds numbers. Fig. 11 shows the liquid film thickness of the oval-shaped tube at different intertube spacing at $Re = 800$. The film thickness increases with the decrease of intertube spacing. The change of film thickness is apparent due to the impact effect at the top region of the tube, while with fluid flowing by, the effect of intertube

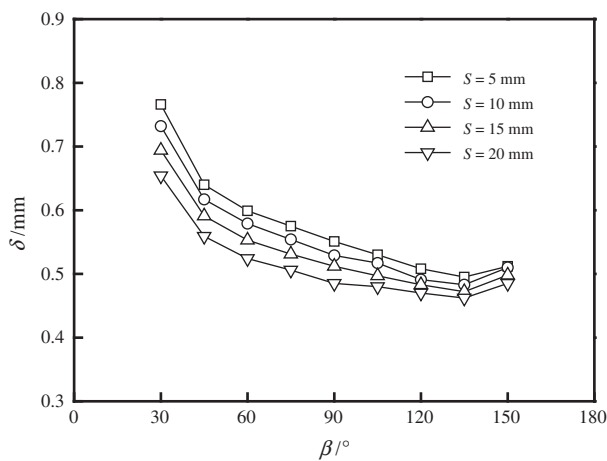


Fig. 11. Variations of film thickness of the oval-shaped tube for different intertube spacing ($Re = 800$).

spacing becomes less evident on film thickness. According to Fig. 11, the minimum value of the film thickness appears approximately at the angular position of 135° .

A comparison of the film thickness for the oval-shaped and circular tube at Reynolds number of approximately 400 and 2000 are plotted against the angular position in Fig. 12. The results are agreed with the numerical data in the paper of Luo et al. [16]. It can be seen that the film thicknesses increases as the mass flow rate increases for each tube. On the upper semi-circle of the tube, the film thickness of the oval-shaped tube at the same β is larger than that of the circular tube. Taking the condition of Reynolds number of about 400 shown in Fig. 12, for example, the average film thicknesses of the oval-shaped tubes are 7.59% larger than that of the circular tube. The main reason is that the curvature of the upper part of the circular tube is the smallest, and thus the change rate of flow velocity on the surface is the lowest compared with the non-circular tubes under the same flow discharge [17]. At the lower part of the tube, the minimum value of film thickness of the circular tube appears nearly at the angle of 105° . However, the curvatures of the lower part for non-circular tubes are smaller than that of the circular tube, which results in a larger gravity component in the flow direction and a larger flow rate of liquid film. Therefore, the film thickness of non-circular tubes decreases dramatically compared to the circular tube as the angle increases at the lower part of the tube. After the approximate angle of 120° , the film thickness of the shaped tube is smaller than the circular tube. Moreover, the minimum film thickness values of the oval-shaped

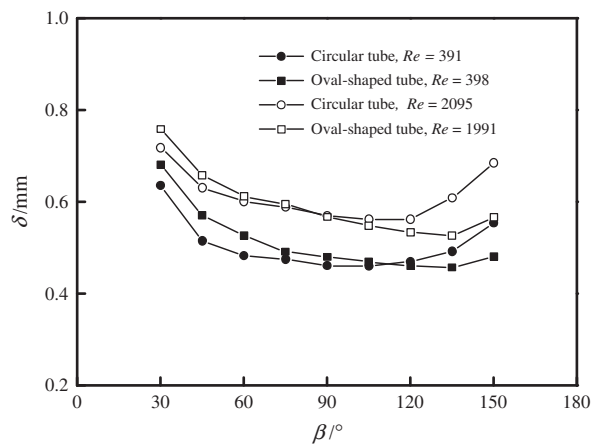


Fig. 12. Variations of film thickness of the oval-shaped tube and circular tube at the given Reynolds numbers ($S = 15$ mm).

tube appear at approximately the angular position of 135°. As shown in Fig. 12, the values of minimum film thicknesses of the oval-shaped tubes are 6.41% smaller than that of the circular tube at a Reynolds number of about 2,000 and at an intertube spacing of 15 mm. Accordingly, there is a probability to gain the optimal tube cross-section, which effectively improves the liquid film distribution and is conducive to obtain the thin liquid film.

Then, the measured values of the circular tube were compared with the predicted values from Eq. (7). The comparison shows that the mean deviation between the measured values and the predicted values is about 15.78%. It indicated that this semi-empiri-

cal correlation is not quite suitable for predicting the measured values due to the difference of the measurement condition and the accuracy of the predicted value. A regression analysis was conducted to develop a correlation for the circular and oval-shaped tube, respectively. In the correlation, the intertube spacing effect on the film thickness is also accounted for by the dimensionless parameter S^* , and are defined as $S^* = S/\zeta$. Based on the correlation of Rogers and Goindi [13], two empirical correlations were obtained for the circular and oval-shaped tube, and are, respectively, written as:

$$\left(\frac{\delta}{d}\right)_{\min} Ar^{1/3} = 5.091 Re^{0.1212} (S^*)^{-0.0590} \tag{9}$$

$$\left(\frac{\delta}{d}\right)_{\min} Ar^{1/3} = 6.037 Re^{0.0883} (S^*)^{-0.0384} \tag{10}$$

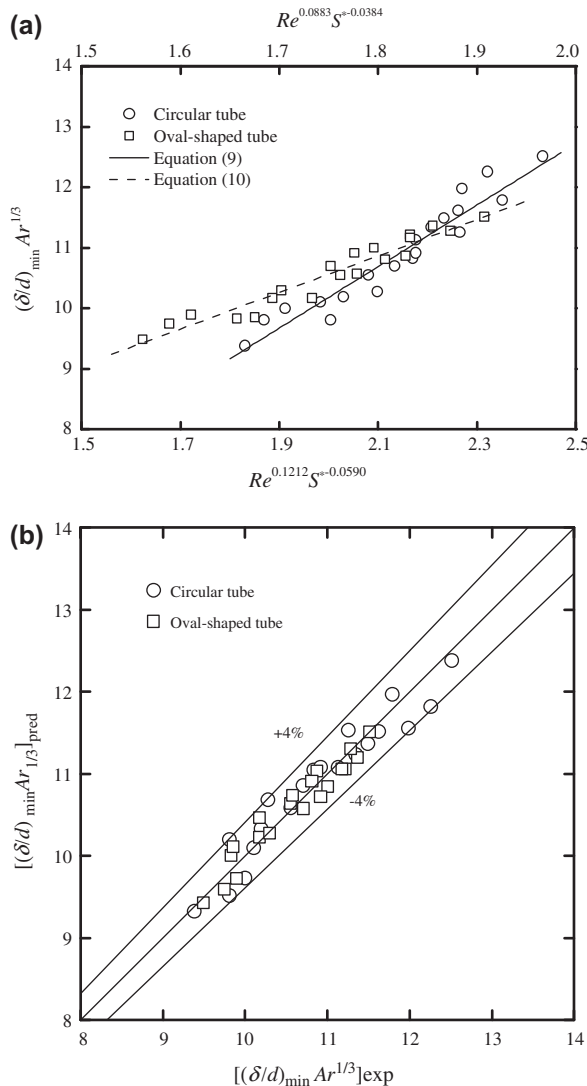


Fig. 13. Comparison of measured film thickness values for circular tube with predicted values from Eqs. (9) and (10).

Fig. 13 shows the comparison between the measured values and the predicted values from Eqs. (9) and (10), with the maximum relative error is within 4 and 3% for the circular and oval-shaped tube, respectively. The results show that Eqs. (9) and (10) has better predictive validity for the present experimental data with better linearity compared with Eq. (7).

5. Conclusions

In this paper, an experimental analysis has been presented for the effect of the oval-shaped tube on the flow characteristics of liquid falling film on the horizontal tube bundle, including mode transition, falling film wavelength, and film thickness. From the experimental results and the discussion of the present study, the following conclusions can be obtained.

- (1) The flow modes on the oval-shaped tube are similar to those on the circular tube, that is, the sheet, sheet-jet, jet, jet-droplet, and the droplet mode with the decrease of film Reynolds number. The intertube spacing has an important role in the flow mode transition. The study showed that the mode transition starts early (at lower Reynolds number) by using the oval-shaped tube.
- (2) The falling dimensionless wavelength increases with the decrease of Reynolds number and firstly increases then tends towards stability with increasing of intertube spacing. The study found that the falling wavelength of the oval-shaped tube is smaller than that of the circular tube by 6.66% at an intertube spacing of 5 mm.
- (3) The film thickness increases with the increase of

Reynolds number and the increasing trend of the film thickness decreases gradually. The film thickness of the oval-shaped tube is larger than the circular tube on the upper part of the horizontal tube, while it is smaller on the lower part of the horizontal tube. The thinnest liquid film appears at approximately the angular position of 105°, and 135° for the circular and oval-shaped tube, respectively. It is found that the minimum film thicknesses of the oval-shaped tube are 6.41% less than that of the circular tube, with the Reynolds number at about 2,000 and intertube spacing of 15 mm.

- (4) The inference can be drawn in such a way that optimization of the cross-section of horizontal tubes will be effectively helpful to the improvement of flow mode and film distribution of falling film flow.

Acknowledgments

The authors gratefully acknowledge the support of the Shandong Province Key Scientific and Technological Project (grant no. 2008GG10007009) and Science and Technology Development Planning of Shandong Province China (grant no. 2012GGX10421).

List of symbols

A	— radius of upper semi-circle tubes, m
Ar	— archimedes number, $g\rho^2d^3/\mu^2$
b	— radius of bottom semi-circle for drop-shaped tube; ellipse semi-major axis, m
d	— tube diameter, m
g	— gravity acceleration, m s^{-2}
Ga	— galileo number, $\rho\sigma^3/(g\mu^4)$
r	— radius of curved surface, m
Re	— reynolds number, $4/\mu$
T	— temperature, °C
S	— intertube spacing, m
u	— velocity component in x -direction, m s^{-1}
v	— velocity component in y -direction, m s^{-1}
x	— coordinate along the body surface, m
y	— coordinate normal to the surface, m

Greek symbols

Γ	— mass flow rate per unit length on each side, $\text{kg m}^{-1} \text{s}^{-1}$
δ	— film thickness, m
β	— polar angle, deg or rad
μ	— dynamic viscosity, $\text{kg m}^{-1} \text{s}^{-1}$
ρ	— density, kg m^{-3}
σ	— liquid surface tension, N m^{-1}
λ	— thermal conductivity, $\text{W m}^{-1} \text{K}^{-1}$
ζ	— capillary constant, m

Superscript

* — dimensionless

Subscripts

L — liquid
V — vapor
Min — minimum

References

- [1] A.M.I. Mohamed, Flow behavior of liquid falling film on a horizontal rotating tube, *Exp. Therm. Fluid Sci.* 31 (2007) 325–332.
- [2] J. Mitrovic, Influence of tube spacing and flow rate on heat transfer from a horizontal tube to a falling liquid film, *Proceedings of the 8th International Heat Transfer Conference, San Francisco, CA, (1986) 1949–1956.*
- [3] X. Hu, A.M. Jacobi, The intertube falling film: Part 1—Flow characteristics, mode transitions, and hysteresis, *J. Heat Transfer* 118 (1996) 616–625.
- [4] R.E. Bellman, R. Pennington, Effects of surface tension and viscosity on Taylor instability, *Q. Appl. Math.* (1954) 151–162.
- [5] R. Armbruster, J. Mitrovic, Heat transfer in falling film on a horizontal tube, *ASME-PUBLICATIONS-HTD* 314 (1995) 13–22.
- [6] A.M.I. Mohamed, Experimental study of heat transfer and flow characteristics of liquid falling film on a horizontal fluted tube, *Heat Mass Transfer* 46 (2010) 841–849.
- [7] X. Hu, A.M. Jacobi, Departure-site spacing for liquid droplets and jets falling between horizontal circular tubes, *Exp. Therm. Fluid Sci.* 16 (1998) 322–331.
- [8] D. Maron-Moalem, S. Sideman, A.E. Dukler, Dripping characteristics in a horizontal tube film evaporator, *Desalination* 27 (1978) 117–127.
- [9] H.-S. Chung, K. Wusiman, S.-S. Kim, B. Nasan, H. Afrianto, H. Rehman, D.-Y. Choi, H.-M. Jeong, Liquid film falling behaviour on horizontal circular cylinder, *J. Cent. South Univ. Technol.* 19 (2012) 1353–1358.
- [10] X.F. Wang, P. Hrnjak, S. Elbel, A. Jacobi, M. He, Flow modes and mode transitions for falling films on flat tubes, *J. Heat Transfer* 134 (2012) 021801.
- [11] X.F. Wang, M.G. He, K. Lv, H.L. Fan, A.M. Jacobi, Effects of liquid supply method on falling-film mode transitions on horizontal tubes, *Heat Transfer Eng.* 34 (2012) 562–579.
- [12] W. Nusselt, Surface condensation of water vapour, *Z. Vereines Deut. Ingenieure* 60 (1916) 541–546.
- [13] J. Rogers, S. Goindi, Experimental laminar falling film heat transfer coefficients on a large diameter horizontal tube, *Can. J. Chem. Eng.* 67 (1989) 560–568.
- [14] L.C. Luo, G.M. Zhang, J.H. Pan, M.C. Tian, Flow and heat transfer characteristics of falling water film on horizontal circular and non-circular cylinders, *J. Hydrodyn., Ser. B* 25 (2013) 404–414.

- [15] H. Hou, Q. Bi, H. Ma, G. Wu, Distribution characteristics of falling film thickness around a horizontal tube, *Desalination* 285 (2012) 393–398.
- [16] L.C. Luo, G.M. Zhang, M.C. Tian, J.H. Pan, Numerical simulation of liquid film flow on horizontal circular and shaped cylinders for falling film evaporation, (*J. Eng. Thermophys.*) *Kung Cheng Je Wu Li Hsueh Pao* 34 (2013) 710–714 (in Chinese with English abstract).
- [17] Q.G. Qiu, J.B. Chen, Numerical simulation of film formation on horizontal-tube falling film evaporators, (*J. Chin. Soc. Power Eng.*) *Dongli Gongcheng Xuebao* 31 (2011) 357–361, 374 (in Chinese with English abstract).